Parametric Oscillators and Soliton Combs in Bandgap-detuned Nanoresonators

Yan Jin[1,2], Jizhao Zang[1,2], Travis Briles[1], David Carlson[1,3], Scott Papp[1,2]
[1]Time and Frequency Division, National Institute of Standards and Technology, Boulder, Colorado, USA
[2]Department of Physics, University of Colorado, Boulder, Colorado, USA
[3]Octave Photonics, Louisville, Colorado, USA
yan.jin@colorado.edu

Abstract: We report controllable generation of OPO lasers and soliton microcombs by manipulating nonlinear dynamics with nanophotonic bandgaps. By excitation detuned from bandgap modes, we realize wide-tunability, low-threshold-power and high-conversion-efficiency lasers.

1. Introduction

The capability to generate laser sources with a nearly arbitrary spectrum and quantum-limited noise properties is a fundamental challenge for integrated photonics that supports applications ranging across science, optical communication [1], spectroscopy [2], and quantum technologies [3]. Kerr-nonlinear microresonators convert an input pump laser into a new source, according to the phase-matching condition for four-wave mixing in the presence of the intraresonator pump field and group-velocity dispersion [4]. Optical parametric oscillation (OPO) lasers [5] and microcombs [6] are key examples. Hence, detailed control of dispersion in microresonators offers an opportunity to engineer new laser sources. While changing the waveguide geometry of a microresonator is a well-established technique, OPO lasers and microcombs require discrete, mode-by-mode frequency control to fully balance nonlinear frequency shifts associated with generating new sources [7,8]. Indeed, by use of coherent scattering with sub-wavelength structures, we have opened up dispersion control for discrete modes. Kerr resonators with such meta-dispersion design provide new opportunities to control the nonlinear dynamics of optical states, including OPO lasers, microcombs, and even generation of quantum states in integrated photonics [9,10].

We create photonic-crystal ring resonators (PhCRs) by nano-patterning the waveguide that forms a microresonator with lithography and dry chemical etching. In the PhCR, coherent scattering couples forward and backward propagation of the resonator mode that corresponds to the periodicity of the nanopattern. Specifically, the PhCR features a highly controllable optical bandgap or frequency splitting on one (or many) modes that can be used to implement complex dispersion behaviors of the resonator mode spectrum. Recent work has shown that pumping a frequency-split mode enables high-efficiency OPOs [11], solitons [7] and exotic microcomb dynamics [8], but it also induces certain limitations, including a conversion efficiency penalty, higher threshold power requirements, and the emission of newly generated laser sources in the backward direction in reverse of the pump. For integrated-photonics systems, backwards propagation is undesired due to the lack of high-efficiency integrated optical circulators to access the newly generated laser.

Here, we explore generation of OPO lasers and microcombs in PhCRs in which we open optical bangaps on resonator modes that are not excited by the pump laser. Indeed, operating PhCRs in this bandgap-detuned regime enables us to balance Kerr shifts in new generation of laser sources without perturbing the intraresonator pump laser field. We report generation of OPO lasers and microcombs with predominant emission in the forward direction. Moreover, these devices operate with low threshold power and high pump-to-comb efficiency, since the pump and new laser sources are propagating in the forward direction. We achieve forward efficiency up to 48% for OPOs, and 37% for soliton microcombs. Our approach paves the way for practical application of forward-propagating, high-efficiency OPOs and microcombs in high-speed optical interconnects.

2. Experimental setup and OPO generation

As shown in Fig. 1(a), a PhCR can be seen as a 3-port system with model fields A_μ which propagate in the forward direction, and the "loss" to the backward-propagating fields B_μ. The backward fields B_μ are induced by the scattering of the photonic crystal, which is a periodic nanostructure on the inner wall of the ring resonator. This photonic crystal gives rise to a red-shifted mode and a blue-shifted mode with a bandgap $2\Gamma_\mu$ at the designed mode μ so that the resonances follow the integrated dispersion $D_{int}(\mu) \equiv \omega_\mu - \omega_0 - \mu D_1 = D_2\mu^2/2 \pm \Gamma_\mu$, where ω_μ is the resonant frequencies of the ring resonator, ω_0 is the pump frequency, $\mathrm{FSR} = D_1/2\pi$ is the free spectral range, and D_2 is the second order dispersion coefficient. For convenience, we refer to the mode number where $\Gamma_\mu \neq 0$ as μ_s, such that $\Gamma_{\mu_s} \neq 0$ and $\Gamma_{\mu\neq\mu_s} = 0$. Figure 1(b) presents the experimental setup for generation and characterization of OPOs and soliton microcombs. The pump field is provided by a continuous-wave (CW) laser and amplified by an erbium-doped fiber amplifier (EDFA) and sent into the Tantala ($\mathrm{Ta_2O_5}$) microresonator. The circulator separates the forward-propagating pump and the backward-propagating combs. Both the forward- and backward- propagating combs are measured by an optical spectrum analyzer (OSA), and the electrical spectrum analyzer (ESA) is used to measure the relative intensity noise of the forward combs.

Figure 1(c) presents the forward efficiency for two different devices indicated in blue and green, respectively. In the experiment, the split mode is fixed in frequency, and we change the pump mode frequency so that the relative mode number μ_s between the pump mode and the split mode varies. As μ_s changes, the efficiency remains high. The simulated efficiency (solid lines) fits the experimental efficiency (dots) well, which indicates the tunability of our OPOs. Fig. 1(d) and (e) show some examples of forward-propagating spectra for different μ_s. The comb line for the split mode is marked with a green triangle, the pump mode is marked with a red circle, and the other mode at $\mu = -\mu_s$ is marked with a purple square. As the pump frequency varies, the signal doesn't change due to the fixed split mode frequency, but the idler will move accordingly. The pump mode is so highly depleted that it is even lower than the signal and idler, which indicates the high conversion efficiency of our OPOs.

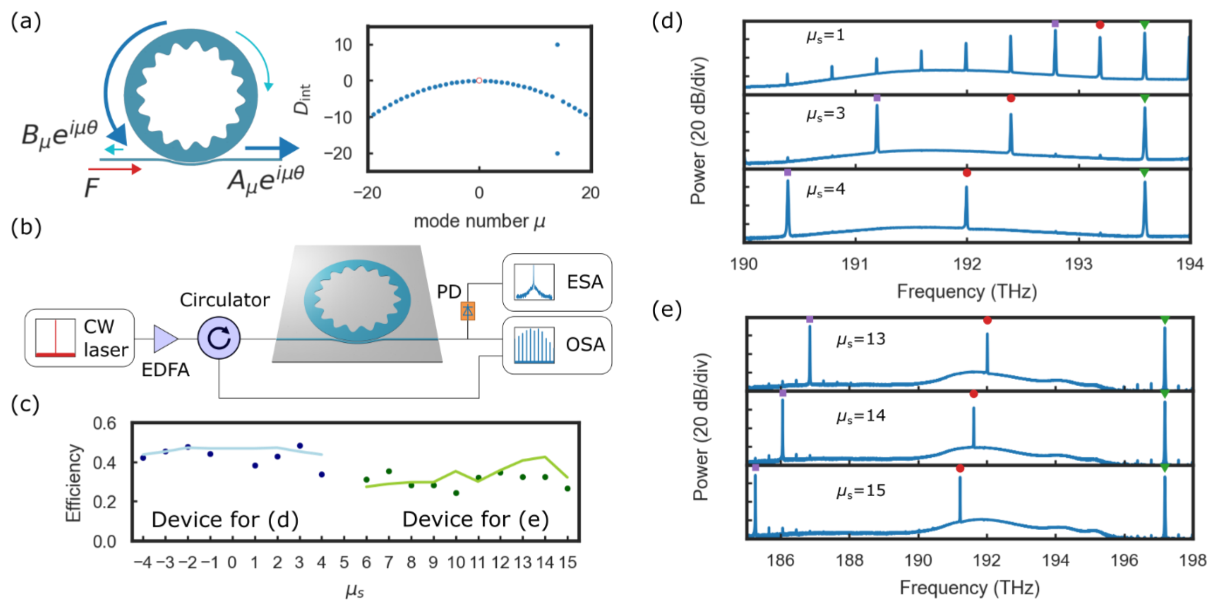

Fig. 1 (a) A schematic diagram of the photonic-crystal microresonator and integrated dispersion for OPO generation. (b) Experimental setup for both OPO and comb generation and characterization. PD, photodiode. (c) Efficiency in the forward direction for two different devices (blue and green). Dots and lines are measured and simulated efficiency, respectively. (d) narrow-band OPO spectra. (e) broad-band OPO spectra.

3. Soliton generation in a PhCR with normal dispersion

Figure 2 presents the principle of dark soliton generation in the bandgap-detuned regime of a PhCR with background normal dispersion. Instead of only splitting one mode, we use 2 split modes at $\mu_s = \pm 1$. This causes an interference pattern on the ring resonator, as shown in the cartoon of Fig. 2(a). A finer structure of the photonic-crystal ring resonator is shown in the scanning electron microscope (SEM) images in Fig. 2(b). The outer wall of the ring is a pure circle, while the inner wall of the ring is modulated by the photonic crystals. Fig. 2(c) presents the measured D_{int} with respect to frequency. According to the measurement, $\Gamma_1 = 0.57$ GHz, $\Gamma_{-1} = 0.47$ GHz and $\Gamma_{\mu\neq\pm1} = 0$. The free spectral range FSR $= D_1/2\pi =$397.848 GHz, and $D_2/2\pi = -12.3$ GHz.

To gain insight into the dynamics of the system, we analyze a modified form of the Lugiato-Lefever equation (LLE) [12]. We characterize soliton phase matching by considering the mode-dependent effective dispersion, $\widetilde{D}_{int}(\mu)$. It is defined as $\widetilde{D}_{int}(\mu) = Re\left(i\dot{A}_\mu/A_\mu\right)$ where the forward electric field A_μ is in the rotating frame of D_1 at mode μ. In the cold cavity, where the pump power is less than threshold $F \ll 1$, the effective $\widetilde{D}_{int}(\mu)$ reduces to the $D_{int}(\mu)$ but with the PhC mode splitting, $\widetilde{D}_{int}(\mu) = D_2\mu^2/2 \pm \Gamma_\mu$. In the hot cavity with pump laser above threshold and with soliton generation, normal dispersion is compensated by the Kerr shift and $\widetilde{D}_{int}(\mu)$ is on a straight line with respect to μ; see Fig. 2(a). Here the effective integrated dispersion can be expressed as $\widetilde{D}_{int}(\mu) = \mu\delta D_1 = 2\pi\mu\left(f_{rep} - \text{FSR}\right)$, where f_{rep} is the repetition rate of the comb lines. The orange dashed line in Fig. 2(a) has a positive slope, indicating f_{rep}>FSR. In the experiment, the measured $f_{rep} = 397.869$ GHz, which is 21 MHz greater than FSR, which agrees with our prediction. $\widetilde{D}_{int}(\mu) \neq 0$ is due to the difference between the two bandgaps $\Gamma_{\pm 1}$. This difference directly leads to asymmetric comb shape, which is verified by both the experiment and the simulation.

Figure 2(e) presents the experimental (solid) and simulated (orange) spectra in the forward ($|A_\mu|^2$) and backward ($|B_\mu|^2$) direction. It shows a good agreement between the experiment and the simulation. In $|B_\mu|^2$, only modes at $\pm 1, \pm 3, \pm 5$ ... occur in simulation. The other lines pop up in experiments because there's reflection from the end of our waveguide. The efficiencies of the forward and backward combs are 37% and 11%, respectively, which verifies the forward propagating feature in the bandgap-detuned excitation regime. Despite the asymmetry of the combs, the simulated temporal fields in Fig. 2(f) still indicate dark soliton generation in the ring resonator.

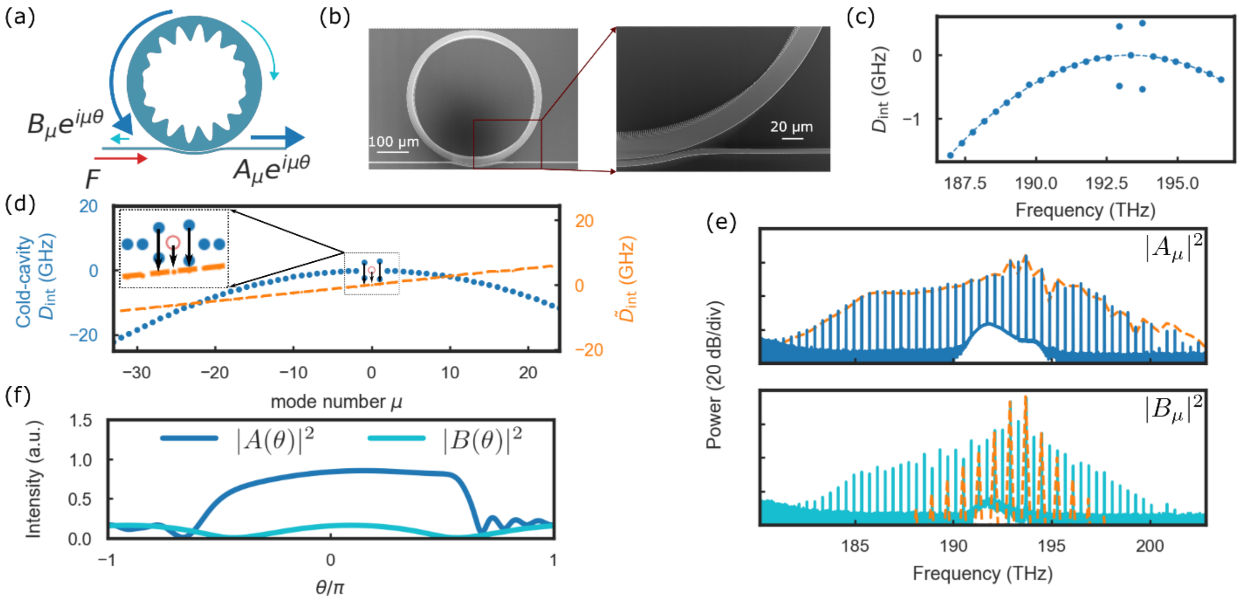

Fig. 2 (a) A schematic diagram for dark soliton generation. (b) SEM images. (c) Experimentally measured $\boldsymbol{D_{int}}$. (d) Phase matching diagram. (e) Experimental and simulated spectra in the forward and backward direction. (f) Simulated forward and backward temporal pulse in the ring coordinate $\boldsymbol{\theta}$.

4. Conclusion

In summary, we experimentally demonstrate the forward-propagating high-efficiency OPO and dark soliton generation in the bandgap-detuned regime. For OPOs, we achieve broad-band frequency tunability and conversion efficiency up to 48%. For dark solitons, we split 2 modes around the pump mode using the special photonic-crystal design. With controlled loss to the backward direction, our soliton reaches the efficiency of 37% in the forward direction, and around 46% for the total. Our work represents an important step towards forward-propagating high-efficiency OPO lasers and soliton microcombs.

References

[1] Yang, K.Y., Shirpurkar, C., White, A.D. et al. “Multi-dimensional data transmission using inverse-designed silicon photonics and microcombs.” Nat Commun 13, 7862 (2022).
[2] M. T. Hummon, et al. “Photonic chip for laser stabilization to an atomic vapor with 10−11 instability,” Optica 5, 443–449 (2018).
[3] Kirchmair, G., et al. “Observation of quantum state collapse and revival due to the single-photon Kerr effect.” Nature 495, 205–209 (2013).
[4] Briles, T., et al. "Interlocking Kerr-microresonator frequency combs for microwave to optical synthesis." Opt. Lett. 43, 2933-2936 (2018).
[5] Lu, X., et al. "Milliwatt-threshold visible–telecom optical parametric oscillation using silicon nanophotonics." Optica 6, 1535-1541 (2019).
[6] Tobias J. Kippenberg et al. “Dissipative Kerr solitons in optical microresonators.” Science 361, eaan8083(2018).
[7] Yu, S.-P., Cole, D.C. et al. “Spontaneous pulse formation in edgeless photonic crystal resonators”. Nature Photonics 15, 461–467 (2021)
[8] Lucas, E., et al. “Tailoring microcombs with inversedesigned, meta-dispersion microresonators.” Nature Photonics, 1–8 (2023).
[9] Joshi, C. et al. “Frequency-Domain Quantum Interference with Correlated Photons from an Integrated Microresonator.” PhysRevLett.124.143601 (2020).
[10] Yang, Z., Jahanbozorgi, M., Jeong, D. et al. “A squeezed quantum microcomb on a chip.” Nat Commun 12, 4781 (2021).
[11] Jennifer A. Black, et al. "Optical-parametric oscillation in photonic-crystal ring resonators." Optica 9, 1183-1189 (2022)
[12] Kondratiev, N.M., Lobanov, V.E. “Modulational instability and frequency combs in whisperinggallery-mode microresonators with backscattering.” Physcal Review A 101, 013816 (2020).